Dominance of Wildfires Impact on Air Quality Exceedances during the 2020 Record-Breaking Wildfire Season in the United States

Yunyao Li[1], Daniel Tong[1,2], Siqi Ma[1], Xiaoyang Zhang[3], Shobha Kundragunta[4], Fangjun Li[3,] Rick Saylor[5]

[1] Department of Atmospheric, Oceanic and Earth Sciences, George Mason University, Fairfax, VA, USA

[2] Center for Spatial Information Science and Systems, George Mason University, Fairfax, VA, USA

[3] Geospatial Sciences Center of Excellence, Department of Geography & Geospatial Sciences, South Dakota State University, Brookings, SD, USA

[4] NOAA Satellite Meteorology and Climatology Division, College Park, MD, USA

[5] NOAA Air Resources Laboratory, College Park, MD, USA

Corresponding author: Yunyao Li (yli74@gmu.edu) and Daniel Q. Tong (qtong@gmu.edu)

Key Points:

- Wildfire emissions contribute 42% of surface $PM_{2.5}$ concentration in the contiguous United States during the summer of 2020;
- Wildfires were the primary contributor to the 3,720 exceedances of National Ambient Air Quality Standard for $PM_{2.5}$ during the 2020 summer;
- Our finding highlights the predominating influence of wildfires on air quality during the 2020 wildfire season.

Key words:

Biomass burning; aerosol; emission; air quality; exceedance; CMAQ

Abstract

The western United States experienced a record-breaking wildfire season in 2020. This study quantifies the contribution of wildfire emissions to the exceedances of health-based National Ambient Air Quality Standard (NAAQS) for fine particles ($PM_{2.5}$) by comparing two CMAQ simulations, with and without wildfire emissions. During August to October 2020, western wildfires contributed 23% of surface $PM_{2.5}$ in the contiguous US (CONUS), with a larger contribution in Pacific Coast (43%) and Mountain Region (42%). Consequently, wildfires were the primary contributor to the 3,720 observed exceedances. The wildfire influence peaked on September 14^{th}, 2020, when 273 exceedances were recorded

and wildfire emissions contributed 41%, 81%, and 72% to surface $PM_{2.5}$ concentrations in the CONUS, Pacific Coast, and Mountain regions, respectively. Our finding highlights the predominating influence of wildfires on air quality, and potentially human health, that is expected to grow with increasing fire activities, while anthropogenic emissions decrease.

Plain language summary

In the summer of 2020, the western United States experienced a record-breaking number of wildfires. We looked into the effects of these wildfires on air quality, through the lens of the exceedances of health-based National Ambient Air Quality Standards (NAAQS) for fine particles ($PM_{2.5}$), which are associated with the bulk of health risks posed by air pollution. We found that in 2020, the western wildfires contributed 23% of surface $PM_{2.5}$ pollution during August to October in the contiguous United States. The contribution is much bigger in the Pacific Coast (43%) and the Mountain region (42%). Consequently, the wildfires were the primary contributor to the 3,720 exceedances of $PM_{2.5}$ NAAQS. Our finding highlights the dominating influence of wildfire emissions on air quality and potentially on human health.

1 Introduction

Biomass burning (BB) emits a large quantity of aerosols and trace gases into the atmosphere, often leading to hazardous air quality and health problems (Koning, et al., 1985). In the summer of 2020, the western United States experienced a record-breaking wildfire season. A series of large wildfires, fueled by accumulated biomass, heatwaves, and dry winds, burned more than 10.2 million acres. These wildfires spread rapidly and destroyed several small towns in California, Oregon, and Washington. According to MODIS (Moderate Resolution Imaging Spectroradiometer) measured FRP (fire radiative power) from 2002 to 2020 (Figure 1a), the monthly total FRP in September 2020 (red star) over the contiguous United States (CONUS) is the highest in over the past 19 years and is more than twice as large as the second highest. Dense wildfire smoke also produced hazardous air quality that affected millions of people in major cities for weeks. Based on Suomi NPP VIIRS (Visible Infrared Imaging Radiometer Suit) 550 nm aerosol optical depth (AOD) measurements, the fire smoke was transported across the continent to the eastern U. S. coast via the westerlies in the middle of September (Figure 1b).

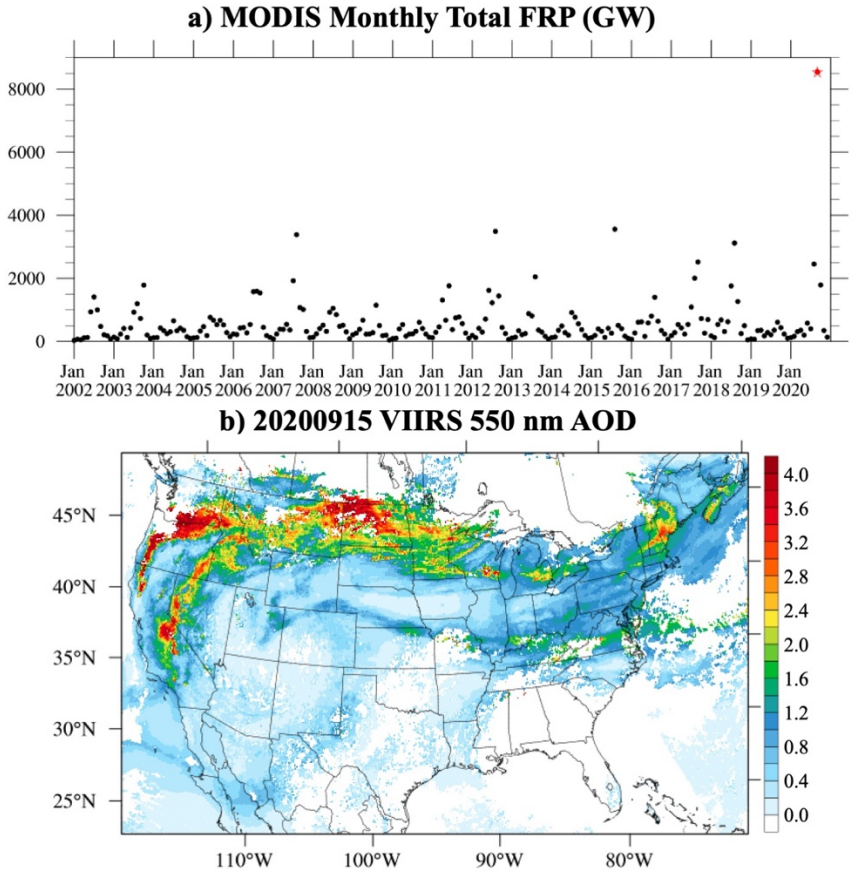

Figure 1. a) MODIS measured monthly total FRP (GW) over the US from January 2002 to September 2020; b) VIIRS measured 550 nm AOD on September 15, 2020.

To protect human health and the environment, the National Ambient Air Quality Standards (NAAQS) have been established for seven criteria air pollutants (CAPs), which includes carbon monoxide (CO), ozone (O_3), particulate matter (PM), nitrogen dioxide (NO_2), and sulfur dioxide (SO_2) that can be emitted or formed by biomass burning. Among these CAPs, $PM_{2.5}$ (PM with aerodynamic diameter of 2.5 micrometers or less) is of particular concern. The Global Burden of Disease comparative risk assessment attributed 3.2 million premature deaths worldwide to human exposure to ambient $PM_{2.5}$ in 2010, which is much greater than other air pollutants or some well-known health threats (e.g., malaria, HIV-AIDS, etc.) (Lim et al., 2012). Currently, the U.S. Environmental Protection Agency (EPA) has primary and secondary standards for $PM_{2.5}$ (annual average standards with levels of 12.0 $\mu g/m^3$ and 15.0 $\mu g/m^3$, respectively; 24-hour standards with 98^{th} percentile forms and levels of 35 $\mu g/m^3$) (U.S. EPA, 2021). The EPA also employs the Exceptional Events Rule for unusual or naturally

occurring events (i.e., wildfire, high wind dust events, etc.), so that air quality data influenced by these sources can be excluded to determine exceedances of NAAQS.

This study aims to assess the air quality impact of the record-breaking wildfires in 2020, with a focus on exceedances of the NAAQS for $PM_{2.5}$. We use the George Mason University (GMU) wildfire forecast system (section 2.2) that relies on satellite estimates of biomass burning emissions and the Community Multiscale Air Quality Modeling System (CMAQ) to simulate emission, transport, and transformation of smoke $PM_{2.5}$ during the 2020 summer wildfire season. The prediction and evolution of wildfire plumes and their impact on air quality is very challenging due to large uncertainties in wildfire emissions (Pereira et al., 2016; Pan et al., 2020), estimation of plume rise (Briggs 1969; Freitas et al., 2007; Stein et al., 2009; Rio et al., 2010; Sofiev et al., 2012; Paugam et al., 2016; Vernon et al., 2018; Zhu et al., 2018), meteorological fields, and chemical transport processes (Li et al., 2019; Li et al., 2020). The BB emissions product used in this study is the blended Global Biomass Burning Emissions Product from MODIS and VIIRS (GBBEPx V3, Zhang et al., 2012, 2019). To enhance the modeling system's capability to predict wildfire smoke, we have implemented a new plume rise scheme based on the algorithm proposed by Sofiev et al. (2012) into the CMAQ model. The current plume rise scheme in CMAQ is based on Briggs (1969), which was originally designed for simulating plumes from well-defined sources such as power plants in a non-disturbed atmosphere. The Sofiev scheme utilizes fire radiative power (FRP), planetary boundary layer (PBL) height, and the Brunt-Vaisala frequency in the free troposphere to estimate fire injection height. Both the Sofiev plume rise scheme and the GBBEPx emission products have been shown to perform well during large wildfire events such as the 2018 Camp Fire (Li et al., 2020).

2 Methods and Data

Experiment design

To evaluate the impact of wildfires on air quality, three CMAQ simulations were conducted. In the first run (ALLF), all emissions from wildfires, prescribed fires, and other biomass burning sources are accounted for in the model simulation. In the second run with no fire emissions (NOF), all types of biomass burning emissions are excluded. The third run (WDF) is the same as the ALLF run, but only has western (west of 102° W) U.S. wildfire emissions. In the WDF run, the USGS 24-category land use categories are used to define the location of forests (i.e., deciduous broadleaf forest, deciduous needleleaf forest, evergreen broadleaf, evergreen needleleaf, and mixed forest).

Comparing results from these three simulations will elucidate the impacts of biomass burning, wildfire, and prescribed fires on air quality. The impacts of biomass burning are generated by subtracting the NOF results from ALLF.

Wildfire emission impact is represented by the difference between WDF and NOF, and the impacts from prescribed fires and other burning sources aside from wildfires are illustrated by the difference between ALLF and WDF.

Description of the modeling system

The CMAQ model is a numerical air quality model that simulates the concentration of airborne gases and particles and the deposition of these pollutants. CMAQ V5.3.1 (U.S. EPA, 2019) was employed to simulate the 2020 summer wildfire season from August 1st to October 31st, over the contiguous United States (CONUS) domain. Details about the system setup are shown in Table S1. The model resolution is 12 km with 35 vertical layers. The 12 km Weather Research and Forecasting (WRF; Skamarock et al., 2019) model V4.2 output was used as the meteorology inputs for the CMAQ model. The initial and boundary conditions for WRF are from the Global Data Assimilation System (GDAS) 0.25-degree analysis and forecast. The time step for the simulation was 60 seconds. The main physics choices were the Grell-Freitas scheme (Grell and Freitas, 2016) for parameterized cumulus processes, the Mellor-Yamada-Janjic scheme (Janjic, 1994) for the planetary boundary layer (PBL) processes, the two-moment Morrison microphysics (Morrison et al., 2009) for cloud physics processes, the RRTMG scheme (Iacono et al., 2008) for longwave and shortwave radiation, and the Noah scheme (Koren et al., 1999) for land surface processes.

The initial chemistry conditions on August 1st are from the NOAA operational air quality forecast (https://airquality.weather.gov/). Anthropogenic emissions of nitrogen oxides (NO_x), volatile organic compounds (VOCs), sulfur dioxide (SO_2), carbon monoxide (CO), ammonia (NH_3), and particulate matter were prepared via the 2016v1 Emissions Modeling Platform (Eyth et al., 2020). The emission inventories used in this platform originate from the National Emissions Inventory (NEI) 2014v2 and have been updated to better represent the year 2016. The model-ready emission files are processed and generated by the Sparse Matrix Operator Kennel Emissions (SMOKE) model (Houyoux et al., 2000) V4.7. The CB6 gas-phase chemical mechanism (Luecken et al., 2019), AE07 aerosol scheme, (Xu et al., 2018; Pye et al., 2015) and aqueous chemistry (Fahey et al., 2017) are used in the CMAQ system.

Biomass burning emissions and plume rise treatment

The GBBEPx biomass burning emission data (Zhang et al., 2012, 2014, 2019) are used as the fire emission input for the CMAQ model.

To achieve a better simulation of fire plumes, a new plume rise scheme was added to the CMAQ model – the Sofiev et al. (2012) scheme that utilizes FRP, PBL height (H_{PBL}), and the Brunt-Vaisala (BV) frequency in the free troposphere to estimate the plume injection height (H_p) for wild-land fires:

$$H_p = \alpha H_{\mathrm{PBL}} + \beta \left(\frac{\mathrm{FRP}}{\mathrm{FRP}_0}\right)^{\gamma} \exp\left(-\frac{\delta \mathrm{BV}_{\mathrm{FT}}^2}{\mathrm{BV}_0^2}\right) \quad (1)$$

Where FRP is the daily fire radiative power provided in NOAA GBBEPx V3, FRP_0 is the reference fire power which equals to 106 W, BV_{FT} is the Brunt-Vaisala frequency in the free troposphere (FT), BV_0 is the reference Brunt-Vaisala frequency which equals to 2.5×10^{-4} s^{-2}, and where , , , are constants. The , , , values are based on Sofiev et al. (2012), and Li et al. (2020). For wildfire simulations, the Sofiev scheme is more stable and accurate (Li et al., 2020) than the CMAQ default plume rise scheme, which is the Briggs (1969) scheme designed for chimneys.

Observation data and assessment method

To evaluate the model simulation as well as the wildfire emission impacts, the simulated results are compared to AirNow ground $PM_{2.5}$ observations and VIIRS measured AOD at 550 nm.

The area hit ratio (Kang et al., 2007) is used to evaluate the surface $PM_{2.5}$ simulation. The calculation of area hit is based on observed and simulated $PM_{2.5}$ exceedance. According to EPA NAAAQS (U.S. EPA, 2020), the exceedance level (E) for $PM_{2.5}$ is set to 35 $\mu g/m^3$ for 24-hour $PM_{2.5}$. Area hit (aH) is defined as:

$$aH = \left(\frac{E_{\mathrm{OM}}}{E_{\mathrm{OM}}+E_O}\right) \quad (2)$$

where E_{OM} is the number of exceedances that are both observed and simulated in the 5×5 grid cells centered at the monitor location (Kang et al., 2007). E_O is the number of observed exceedances that are not simulated within the 5×5 grid cells centered at the monitor location.

The Contribution Ratio (CR) and Exceedance Impact Ratio (EIR) are used to discuss the wildfire biomass burning influence:

$$CR = \frac{M_{\mathrm{WDF}}-M_{\mathrm{NOF}}}{M_{\mathrm{WDF}}} \times 100\% \quad (3)$$

$$EIR = \frac{N_{\mathrm{aff}}}{N_{\mathrm{tot}}} \times 100\% \quad (4)$$

where M_{WDF} is the simulation results (i.e., $PM_{2.5}$, AOD) from the WDF (wildfire only) run, M_{NOF} is the result from the NOF (no fire) run, N_{tot} is the number of total grid cells within the study region (i.e., CONUS, different time zones), and N_{aff} is the number of grid cells that are within the unhealthy wildfire-influenced area in the study region. The unhealthy wildfire-influenced area is defined as the place where the simulated 24-hour $PM_{2.5}$ levels from the WDF run is higher than the exceedance level (35 $\mu g/m^3$) and the simulated 24-hour $PM_{2.5}$ from the NOF run is lower than the exceedance level over the same location.

3 Results

3.1 Model evaluation

The first exceedance of the daily $PM_{2.5}$ NAAQS occurred on August 16^{th}, 2020. After October 10^{th}, wildfire emissions began to decrease, with less than ten exceedances after that date. Therefore, the analysis focuses on the period from August 16^{th} to October 10^{th}, 2020. Figure 2a shows the result of the area hit ratio (blue line) for the CMAQ ALLF run. A high area hit ratio represents a good capture of the region impacted by real smoke. The average area hit ratio during this period is 0.68. During the peak pollution days (from September 12^{th} - 16^{th}) when over 200 stations observed $PM_{2.5}$ exceedance (black dash line in Figure 2), the area hit ratios were higher than 0.96 with a maximum of 1.0 on September 13^{th}, 2020. This suggests that the model could predict more than 96% of the observed exceedances when the smoke pollution was at its peak. The minimum area hit ratio was 0 on August 17^{th}, 2020; however, the fire was not intense and there were only three stations that observed $PM_{2.5}$ exceedances on that day. Traditional evaluation metrics are also used to evaluate the model simulation. The correlation between observed and simulated daily $PM_{2.5}$ concentrations for the ALLF run is shown in Figure 2a (red line) with an average of 0.55. The spatial plot of ALLF $PM_{2.5}$ overlaid by AirNow observations on a peak day is shown in Figure 2b. The contour colors are based on the EPA Air Quality Index for $PM_{2.5}$: green for good, yellow for moderate, orange for unhealthy to sensitive groups, red for unhealthy, purple for very unhealthy, and maroon for hazardous. In most places, the observations and simulation match closely with each other, suggesting that the model performs very well. The AOD results are shown in Figure 2c. Our model reproduced the smoke optical depth from the west coast to the east coast observed by VIIRS (Figure 1b). Overall, the model is able to reproduce wildfire smoke dispersion, especially when the fire is intense.

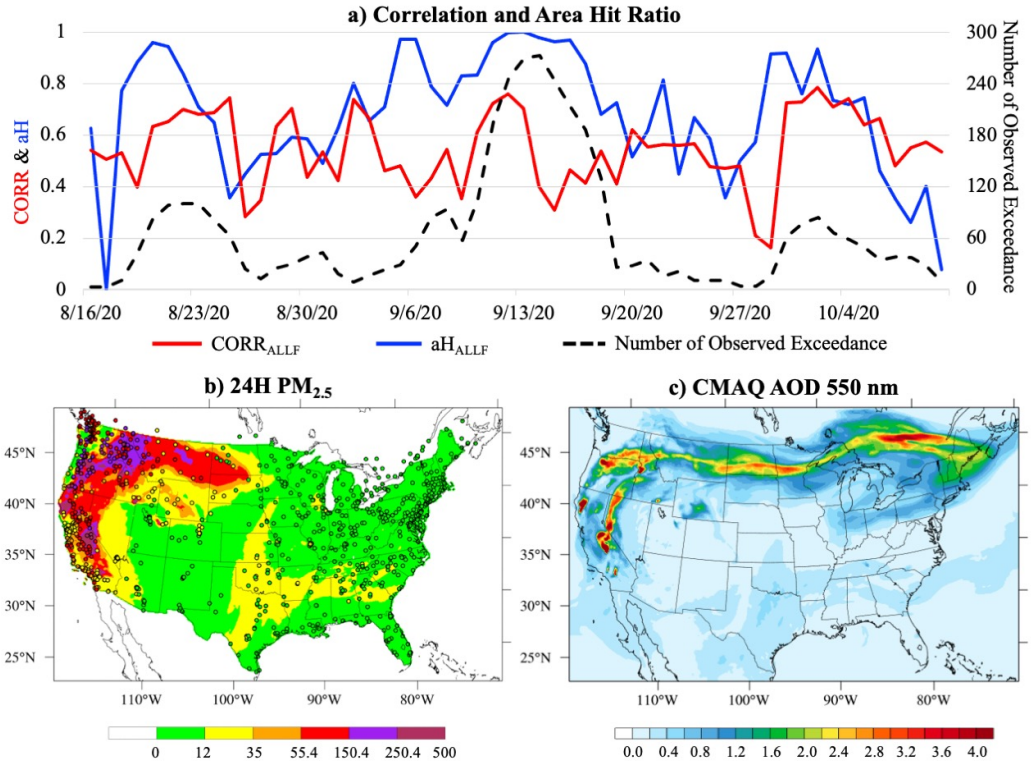

Figure 2. a) Correlation (red) and area hit ratio (blue) between observed and simulated $PM_{2.5}$ from the ALLF run, with the number of observed exceedances (black dash line) from August 16th to October 31st, 2020; b) CMAQ ALLF run for simulated 24-hour $PM_{2.5}$ and overlaid with the AirNow $PM_{2.5}$ observation on September 15th, 2020; c) CMAQ ALLF run for simulated AOD at 550 nm on September 15th, 2020.

Wildfire contribution to $PM_{2.5}$ and AOD

The contribution from wildfires to surface $PM_{2.5}$ concentration is shown Figure 3a. During the analysis period, the West Coast wildfires contributed 23% of surface $PM_{2.5}$ pollution nationwide. Specifically, wildfires produced 43% of the total $PM_{2.5}$ pollutants in the Pacific time zone, 42% in the Mountain time zone, 11% in the Central time zone, and 4% in the Eastern time zone. The $PM_{2.5}$ difference between the WDF run and the NOF run and the wildfire $PM_{2.5}$ CR on September 15, 2020 (one of the peak days) are shown in Figures 3c and 3e. During the peak period, the wildfire $PM_{2.5}$ CRs reached 41% nationwide, 81% in the Pacific time zone, 72% in the Mountain time zone, 33% in the Central time zone, and 10% in the Eastern time zone.

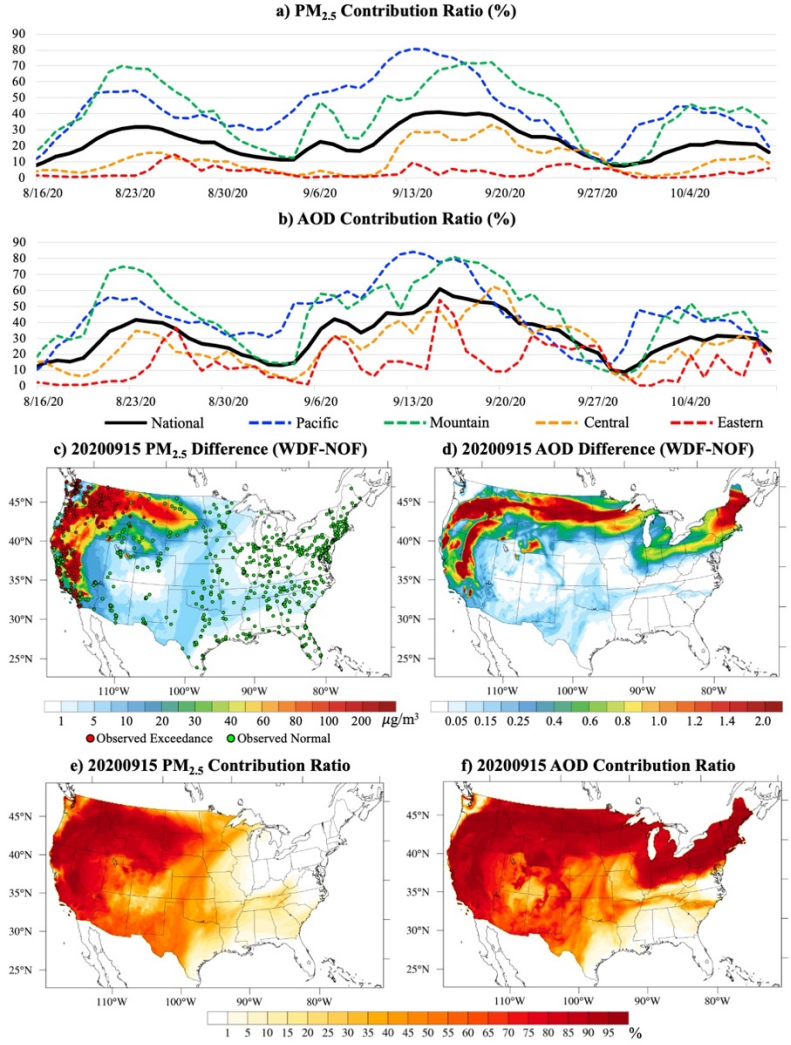

Figure 3. Wildfire $PM_{2.5}$ (a) and AOD (b) contribution ratios; simulation differences between WDF and NOF run on September 15th, 2020, for $PM_{2.5}$ (c, overlaid with observed $PM_{2.5}$ exceedances) and AOD (d); and the wildfire $PM_{2.5}$ (e) and AOD (f) contribution ratio on September 15, 2020.

The thick smoke that originated from California, Oregon, and Washington was transported across the country by the prevailing westerly wind. During September 14-17th, 2020, the fire smoke from the West Coast was transported to the northeastern part of the U.S. (Figures 1b and 2c). While the fire smoke traveled east, it passed 19 states, which included California, Nevada, Oregon, Washington, Idaho, Montana, Wyoming, North Dakota, South Dakota, Minnesota, Wisconsin, Michigan, Pennsylvania, New York, Connecticut, Rhode Island, Mas-

sachusetts, Vermont, New Hampshire, and Maine. The smoke plume was still quite thick when it reached New Hampshire and Maine and had a measured AOD of over 3.

Figure 3b shows the contribution of wildfire emissions to AOD during the study period. The western wildfires contributed an average of 32% to nationwide AOD, 45% in the Pacific Coast, 45% in the Mountain region, 26% in the Central U.S., and 14% in the Eastern United States. On peak days, the wildfire contributed more than 60% of the AOD nationwide, 80% in the Pacific Coast, 80% in the Mountain region, 60% in the Central U.S., and 50% in the Eastern United States. Although the increased AOD resulting from aloft smoke does not have the severe health impacts of surface $PM_{2.5}$, it influences a larger area than surface $PM_{2.5}$ and may affect cloud formation and regional radiative budgets, leading to impacts on regional weather.

Impacts of air quality exceedance caused by wildfires

According to AirNow ground observations, there were 3,720 observed $PM_{2.5}$ exceedances during the analysis period, with an average of 65 exceedances per day and a maximum of 273 exceedances on September 14^{th}, 2020. The observed unhealthy air ($PM_{2.5}$ exceedances, red circles in Figure 3c) crossed seven states in the western U.S., including California, Nevada, Oregon, Washington, Idaho, Montana, and Wyoming. The CMAQ simulations show that the surface smoke might also have extended to the region without ground measurements, such as North Dakota and South Dakota (Figure 3c). The $PM_{2.5}$ exceedances are all located in the areas with large simulated $PM_{2.5}$ differences between the WDF and NOF runs, which indicates that all the observed $PM_{2.5}$ exceedances are caused by wildfire emissions rather than other emissions, such as prescribed burning or other anthropogenic emissions.

The results for wildfire $PM_{2.5}$ national Exceedance Impact Ratio (EIR, eq 4) are shown in Figure 4a. During the peak period, over 18% of surface area nationwide was blanketed in the unhealthy air caused by wildfire smoke. About half of the affected region was located in the Pacific Coast region, and the other half in the Mountain region. Only a few areas in the central or eastern time zone were affected by the surface $PM_{2.5}$ exceedances. The wildfire $PM_{2.5}$ regional EIR for the four time zones are shown in Figure 4b. More than half of the Pacific time zone and one third of the area in the Mountain time zone experienced surface $PM_{2.5}$ exceedances.

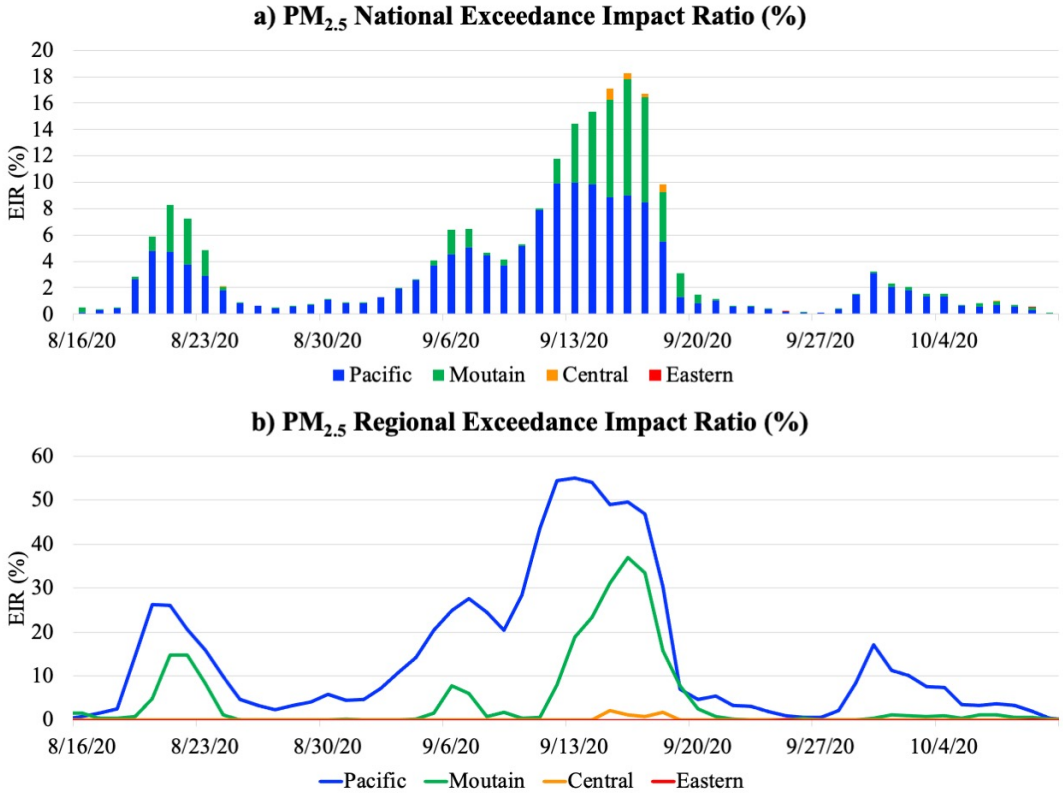

Figure 4. National (a) and Regional (b) wildfire $PM_{2.5}$ Exceedance Impact Ratio (%).

4 Conclusion

In the summer of 2020, the Western United States experienced a record-breaking wildfire season, with the highest FRP in September 2020 in the past 19 years. The CMAQ system with GBBEPx biomass burning and the newly added Sofiev plume rise scheme were used to simulate the 2020 record-breaking wildfire season. The model simulation successfully reproduced the plume dispersion. More than 96% of the polluted area was successfully reproduced during the most polluted days.

From late August to early October, the West Coast wildfires contributed 23% of surface $PM_{2.5}$ pollution nationwide. More than 40% of the $PM_{2.5}$ pollution came from the western wildfires (the Pacific and Mountain time zones). During the peak days, the wildfire contribution to surface $PM_{2.5}$ reached 81% in the Pacific coast, 72% in the inter-Mountain region, and 41% across the entire country. Even in the Eastern time zone, which is far away from the source region, the

model estimates that there is 10% of the total $PM_{2.5}$ pollution came from the West Coast wildfires.

The thick fire smoke that originated in California, Oregon, and Washington was injected into the free troposphere and transported across the country through the prevailing wind, which caused hazy days in 19 states. On the peak days, more than 60% of the nationwide AOD was caused by wildfire emissions. Specifically, 80% in the Pacific and Mountain region, 60% in the Central US, and 50% AOD in the Eastern U.S. were attributed to wildfire plumes. Although the increased AOD caused by the aloft smoke did not have severe health impacts compared to surface $PM_{2.5}$, it influenced a larger area than surface $PM_{2.5}$ and might have further influence on cloud formation and earth radiative budget, which would impact regional weather as well as global climate.

Finally, the West Coast wildfires caused 3,720 observed $PM_{2.5}$ exceedances during the analysis period, with an average of 65 exceedances per day, and a maximum of 273 exceedances on September 14, 2020. The observed unhealthy air ($PM_{2.5}$ exceedances based on the EPA AirNow observations) crossed seven states in the western United States. The surface smoke may also extend to regions where there are no ground measurements in North Dakota and South Dakota based on our CMAQ simulation. During the peak days, over 18% of the CONUS was blanketed by the unhealthy air caused by wildfire smoke. Following research will be conducted on exploring the impacts of wildfire pollution on human health.

Acknowledgement

This work was financially supported by the NOAA Weather Program Office and office of Oceanic and Atmospheric Research (OAR), NASA Health and Air Quality Program, and George Mason University College of Science. The GBBEPx data can be downloaded from https://satepsanone.nesdis.noaa.gov/pub/FIRE/GBBEPx-V3/. The VIIRS measurements can be downloaded from http://air.csiss.gmu.edu/yli/paper_data/viirs/. The AirNow observations can be downloaded from: https://files.airnowtech.org/?prefix=airnow/2020/. The GDAS 0.25-degree analysis and forecast data can be download from https://rda.ucar.edu/datasets/ds083.3/.

Reference

Briggs, G. (1969), Plume rise, Tech. Rep. Crit. Rev. Ser. 81pp., Natl. Tech. Inf. Serv., Springfield, VA.

Eyth, A., Vukovich, J., Farkas, C., & Strum, M. (2020). Technical Support Document (TSD) Preparation of Emissions Inventories for 2016v1 North American Emissions Modeling Platform.

Fahey, K.M., Carlton, A.G., Pye, H.O.T., Baek, J., Hutzell, W.T., Stanier, C.O., Baker, K.R., Appel, K.W., Jaoui, M., & Offenberg, J.H. (2017). A frame-

work for expanding aqueous chemistry in the Community Multiscale Air Quality (CMAQ) model version 5.1. Geoscientific Model Development, 10, 1587-1605. doi: 10.5194/gmd-10-1587-2017

Freitas, S. R., Longo, K. M., Chatfield, R., Latham, D., Silva Dias, M. A. F., Andreae, M. O., Prins, E., Santos, J. C., Gielow, R., & Carvalho, J. A. Jr. (2007). Including the sub-grid scale plume rise of vegetation fires in low resolution atmospheric transport models. Atmospheric Chemistry and Physics, 7(13), 3385– 3398. https://doi.org/10.5194/acp-7-3385-2007

Grell, G. A., & Freitas, S. R. (2014). A scale and aerosol aware stochastic convective parameterization for weather and air quality modeling. Atmospheric Chemistry and Physics, 14(10), 5233–5250. https://doi.org/10.5194/acp-14-5233-2014

Houyoux, M., Vukovich, J., Brandmeyer, J. E., Seppanen, C., & Holland, A. (2000). Sparse matrix operator kernel emissions modeling system-SMOKE User manual. Prepared by MCNC-North Carolina Supercomputing Center, Environmental Programs, Research Triangle Park, NC

Iacono, M. J., Delamere, J. S., Mlawer, E. J., Shephard, M. W., Clough, S. A., & Collins, W. D. (2008). Radiative forcing by long-lived greenhouse gases: Calculations with the AER radiative transfer models. Journal of Geophysical Research, 113, D13103. https://doi.org/10.1029/2008JD009944

Janjić, Z. I. (1994). The Step-Mountain Eta Coordinate Model: Further developments of the convection, viscous sublayer, and turbulence closure schemes. Monthly Weather Review, 122(5), 927–945. https://doi.org/10.1175/1520-0493(1994)122<0927:TSMECM>2.0.CO;2

Kang, D., Mathur, R., Schere, K., Yu, S., & Eder, B. (2007). New Categorical Metrics for Air Quality Model Evaluation. Journal of Applied Meteorology and Climatology, 46(4), 549-555. Retrieved March 1, 2021, from http://www.jstor.org/stable/26171922

Kondragunta, S., Lee, P., McQueen, J., Kittaka, C., Prados, A., Ciren, P., . . . Szykman, J. (2008). Air Quality Forecast Verification Using Satellite Data. Journal of Applied Meteorology and Climatology, 47(2), 425-442. Retrieved March 1, 2021, from http://www.jstor.org/stable/26172156

Koning, H. W., Smith, K. R., & Last, J. M. (1985). Biomass fuel combustion and health, Bulletin of the World Health Organization, 63 (1), 11-26.

Koren, V., Schaake, J., Mitchell, K., Duan, Q.-Y., Chen, F., & Baker, J. M. (1999). A parameterization of snowpack and frozen ground intended for NCEP weather and climate models. Journal of Geophysical Research, 104, 19,569–19,585. https://doi.org/10.1029/1999JD900232

Li, F., Val Martin, M., Andreae, M. O., Arneth, A., Hantson, S., Kaiser, J. W., et al. (2019). Historical (1700–2012) global multi-model estimates of the fire emissions from the Fire Modeling Intercomparison Project

(FireMIP). Atmospheric Chemistry and Physics, 19(19), 12545–12567, https://doi.org/10.5194/acp-19-12545-2019

Li, Y., Tong, D. Q., Ngan, F., Cohen, M. D., Stein, A. F., Kondragunta, S., et al. (2020). Ensemble $PM_{2.5}$ forecasting during the 2018 Camp Fire event using the HYSPLIT transport and dispersion model. J. Geophys. Res. Atmos: Atmospheres, 125, e2020JD032768. https://doi.org/10.1029/2020JD032768

Lim, S., et al., 2012. A comparative risk assessment of burden of disease and injury attributable to 67 risk factors and risk factor clusters in 21 regions, 1990–2010: A systematic analysis for the Global Burden of Disease Study 2010. Lancet, 2012, 380, 2224– 2260

Luecken, D.J., Yarwood, G., & Hutzell, W.H. (2019). Multipollutant of ozone, reactive nitrogen and HAPs across the continental US with CMAQ-CB6. Atmospheric Environment, 201, 62-72. doi: 10.1016/j.atmosenv.2018.11.060

Morrison, H., Thompson, G., & Tatarskii, V. (2009). Impact of cloud microphysics on the development of trailing Stratiform precipitation in a simulated squall line: Comparison of one- and two-moment schemes. Monthly Weather Review, 137(3), 991–1007. https://doi.org/10.1175/2008MWR2556.1

Pan, X., Ichoku, C., Chin, M., Bian, H., Darmenov, A., Colarco, P., Ellison, L., Kucsera, T., da Silva, A., Wang, J., Oda, T., & Cui, G. (2020). Six global biomass burning emission datasets: Inter-comparison and application in one global aerosol model. Atmospheric Chemistry and Physics, 20(2), 969– 994. https://doi.org/10.5194/acp-20-969-2020

Paugam, R., Wooster, M., Freitas, S., & Val Martin, M. (2016). A review of approaches to estimate wildfire plume injection height within large-scale atmospheric chemical transport models. Atmos. Chem. Phys., 16, 907–925. https://doi.org/10.5194/acp-16-907-2016

Pereir, G., Siqueira, R., Rosário, N., Longo, K., Freitas, S. R., Cardozo, F. S., et al. (2016). Assessment of fire emission inventories during the South American Biomass Burning Analysis (SAMBBA) experiment. Atmos. Chem. Phys., 16, 6961–6975. https://doi.org/10.5194/acp-16-6961-2016

Pye, H.O.T.; Luecken, D.J.; Xu, L.; Boyd, C.M; Ng, N.L.; Baker, K.R.; Ayres, B.R.; Bash, J.O.; Baumann, K.; Carter, W. P.L.; Edgerton, E.; Fry, J.L.; Hutzell, W.T.; Schwede, D.B.; Shepson, P.B., Modeling the current and future roles of particulate organic nitrates in the southerneastern United States. Environ Sci Technol 2015, 49(24), 14195-14203. doi: 10.1021/acs.est.5b03738

Rio, C., Hourdin, F., & Chédin, A. (2010). Numerical simulation of tropospheric injection of biomass burning products by pyro-thermal plumes. Atmospheric Chemistry and Physics, 10(8), 3463– 3478. https://doi.org/10.5194/acp-10-3463-2010

Skamarock, W. C., J. B. Klemp, J. Dudhia, D. O. Gill, Z. Liu, J. Berner, W. Wang, J. G. Powers, M. G. Duda, D. M. Barker, and X.-Y. Huang, 2019: A

Description of the Advanced Research WRF Version 4. NCAR Tech. Note NCAR/TN-556+STR, 145 pp.

doi:10.5065/1dfh-6p97

Sofiev, M., Ermakova, T., & Vankevich, R. (2012). Evaluation of the smoke-injection height from wild-land fires using remote-sensing data. Atmospheric Chemistry and Physics, 12(4), 1995–2006. https://doi.org/10.5194/acp-12-1995-2012

Stein, A. F., Rolph, G. D., Draxler, R. R., Stunder, B., & Ruminski, M. (2009). Verification of the NOAA smoke forecasting system: Model sensitivity to the injection height. Weather and Forecasting, 24(2), 379– 394. https://doi.org/10.1175/2008WAF2222166.1

Environmental Protection Agency (2020). Review of the National Ambient Air Quality Standards for Particulate Matter. Federal Register, 85, December 18, 2020, 82684-82748. Available at: https://www.govinfo.gov/content/pkg/FR-2020-12-18/pdf/2020-27125.pdf

United States Environmental Protection Agency. (2020). CMAQ (Version 5.3.2) [Software]. Available from https://doi.org/10.5281/zenodo.4081737

Vernon, C. J., Bolt, R., Canty, T., & Kahn, R. A. (2018). The impact of MISR-derived injection height initialization on wildfire and volcanic plume dispersion in the HYSPLIT model. Atmos. Meas. Tech., 11, 6289–6307. https://doi.org/10.5194/amt-11-6289-2018

Xu, L., Pye, H. O. T., He, J., Chen, Y. L., Murphy, B. N., Ng, N. L. (2018). Experimental and model estimates of the contributions from biogenic monoterpenes and sesquiterpenes to secondary organic aerosol in the southeastern United States. Atmos. Chem. Phys., 18: 12613-12637. doi: 10.5194/acp-18-12613-2018

Zhang, X., Kondragunta, S., Da Silva, A., Lu, S., Ding, H., Li, F., & Zhu, Y. (2019). The blended global biomass burning emissions product from MODIS and VIIRS observations (GBBEPx) version 3.1, https://www.ospo.noaa.gov/Products/land/gbbepx/docs/GBBEPx_ATBD.pdf

Zhang, X., Kondragunta, S., Ram, J., Schmidt, C., & Huang, H.-C. (2012). Near-real-time global biomass burning emissions product from geostationary satellite constellation. Journal of Geophysical Research: Atmospheres, 117(D14). https://doi.org/10.1029/2012JD017459

Zhang, X., Kondragunta, S., & Roy, D. P. (2014). Interannual variation in biomass burning and fire seasonality derived from geostationary satellite data across the contiguous United States from 1995 to 2011. Journal of Geophysical Research: Biogeosciences, 119(6), 1147–1162. https://doi.org/10.1002/2013JG002518

Zhu, L., Val Martin, M., Gatti, L., Kahn, R., Hecobian, A., & Fischer, E. (2018).

Development and implementation of a new biomass burning emissions injection height scheme (BBEIH v1.0) for the GEOS-Chem model (v9-01-01). Geosci. Model Dev., 11, 4103–4116. https://doi.org/10.5194/gmd-11-4103-2018